Planar and Nonplanar Conformations of (*meso*-Tetraphenylporphinato)nickel(II) in Solution As Inferred from Solution and Solid-State Raman Spectroscopy

Walter Jentzen,*,†,‡ Esko Unger,§ Xing-Zhi Song,†,‡ Song-Ling Jia,†,‡ Ilona Turowska-Tyrk,|| Reinhard Schweitzer-Stenner,§ Wolfgang Dreybrodt,§ W. Robert Scheidt,|| and John A. Shelnutt*,†,‡

Catalysis and Chemical Technologies Department, Sandia National Laboratories, Albuquerque, New Mexico 87185-0710, Department of Chemistry, University of New Mexico, Albuquerque, New Mexico 87131, FB1-Institut für Experimentelle Physik, Universität Bremen, P.O. Box 330440, 28334 Bremen, Germany, and Department of Chemistry and Biochemistry, University of Notre Dame, Notre Dame, Indiana 46556

Received: February 7, 1997; In Final Form: May 21, 1997[⊗]

The coexistence in solution of at least two conformers of (*meso*-tetraphenylporphinato)nickel(II) [Ni(TPP)] is inferred from solution and single-crystal resonance Raman spectra obtained at different temperatures (170 − 297 K) and excitation wavelengths (413.1 and 457.9 nm). The shapes of the structure-sensitive Raman lines ν_8 and ν_2 are clearly asymmetric and change with temperature. These broad lines can be decomposed into at least two sublines, a low-frequency (LF) and a high-frequency (HF) component. In contrast, the corresponding single-crystal Raman lines of the nonplanar structure of Ni(TPP) in the crystal are narrow and symmetric. For the line ν_2, the broad LF subline results from nonplanar conformers and the narrow HF subline arises from a more planar conformer. This assignment is consistent with the observation that the LF subline of ν_2 is more enhanced upon changing the excitation wavelength from 413.1 to 457.9 nm. The selective resonance enhancement is caused by the red shifts of the UV−visible absorption bands and Raman excitation profiles of the nonplanar form. The frequency assignment for the sublines of ν_8 is reversed from that of ν_2 (*i.e.*, the HF subline of ν_8 arises from nonplanar conformers and the LF subline results from a more planar macrocycle). This assignment is based on subline broadness and enhancement behavior using an excitation wavelength located on the red side of the B band. The assignments of the sublines to the nonplanar conformer are also in agreement with the Raman spectra of single crystals in which Ni(TPP) is known from X-ray crystallography to have a predominantly ruffled nonplanar conformation. Specifically, the frequencies of the sublines of ν_8 and ν_2 that are assigned to the nonplanar form in solution closely match the frequencies of Ni(TPP) in the single crystal. We propose two thermodynamic models for the interpretation of the temperature dependence of the intensity ratios of the sublines. A two-state model assumes one planar and one nonplanar conformer in solution. From the slopes in the van't Hoff plots, the nonplanar conformer is energetically favored by about 1.8 kJ mol^{-1} in this model. Since molecular mechanics calculations predict three conformers of Ni(TPP) in solution, we also consider a three-state model. The three structures are two nonplanar structures of purely ruffled (*ruf*) and purely saddled (*sad*) macrocyclic distortions and a planar conformer. In the calculations, the *ruf* conformation is the lowest-energy structure with the planar and *sad* conformers having almost equal higher energies. Assuming this relationship between the energies, but allowing the actual energy separation to vary, the three-state analysis gives the similar result that the *ruf* conformation is stabilized by about 2.3 kJ mol^{-1} with respect to the planar and *sad* conformers.

Introduction

A recent advancement in the structural characterization of the heme groups in proteins has convincingly shown that in many cases the observed nonplanarity of the porphyrin is conserved for proteins belonging to the same functional class.[1,2] The structural conservation is even observed for some proteins like the cytochromes c_3 for which a large natural variation in the amino acid sequence occurs. This finding might be expected since functionally related proteins often share the same class of tertiary structures, especially near the functional domains.[3] On the other hand, similarities in the heme structure may not necessarily follow from the similarities in the tertiary structure if the distortions are functionally insignificant; consequently, the conservation of the nonplanar distortions of the heme group might indicate a mechanism for protein modulation of biological properties. This possibility is further emphasized by the observation that the isolated heme group in solution is almost planar,[4] so that the energy necessary to make the heme group nonplanar must be provided by the surrounding protein.

The degree of nonplanarity apparently depends on a multitude of protein−heme interactions. For example, binding of endogenous and exogenous ligands, van der Waals interactions with nearby amino acid residues, and hydrogen bonding to the porphyrin side chains are all significant contributors in causing nonplanar heme distortions in proteins. The peripheral substitutes are of particular importance when they are covalently bonded to the protein (*e.g.*, the vinyl substituents of *c*-type cytochromes) or when they are hydrogen bonded to nearby amino acid residues (*e.g.*, the propionate substituents). The

* To whom correspondence should be addressed: FAX, 505-272-7077; E-mail, jasheln@unm.edu.
† Sandia National Laboratories.
‡ University of New Mexico.
§ Universität Bremen.
|| University of Notre Dame.
⊗ Abstract published in *Advance ACS Abstracts,* July 15, 1997.

S1089-5639(97)00496-9 CCC: $14.00

protein can also influence the orientation of the substituents and this in turn can influence the conformation of the heme. It is therefore important to fully understand the role of peripheral substituents in determining the nonplanar distortions of porphyrins. In this respect, the combination of X-ray crystallography and resonance Raman spectroscopy has been particularly fruitful in examination of the structure−function relationships in various hemoproteins.[5]

Shelnutt and co-workers[6] have investigated in great detail the effect of differently substituted model compounds on the porphyrin distortions using a combination of X-ray crystallography, molecular mechanics calculations, and resonance Raman spectroscopy. From these studies, it emerges that the type, size, and orientation of the substituents determine the degree and type of nonplanar distortions. In particular, all known four-coordinate porphyrins having only hydrogen atoms as peripheral substituents are nearly planar, including Zn(P), Cu(P), and Ni(P).[7] Ni(P), however, is poised to be nonplanar because its central metal ion is too small for the porphinato core.[7b] As a result, substituents at the periphery of nickel porphine cause nonplanar structures which shorten the metal−nitrogen bonds. Or for less bulky substituents, planar and nonplanar conformations may coexist in solution.

In fact, (2,3,7,8,12,13,17,18-octaethylporphinato)nickel [Ni(OEP)] is an example for which planar and nonplanar conformers coexist in solution.[4,8] The conformers of Ni(OEP) are distinguishable spectroscopically in that they give rise to different frequencies in the single-crystal Raman spectra of the two planar and one nonplanar crystalline forms. That is, the structure-sensitive lines ν_3, ν_{11}, ν_2, ν_{19}, and ν_{10} appear at different frequencies for the planar and nonplanar crystal conformers,[9,10] and lines at both frequencies can be identified in the solution resonance Raman spectra of Ni(OEP).[4,8] Apparently, the ethyl substituents at the C_β positions of Ni(OEP) sterically interact sufficiently to induce the appearance of nonplanar conformers in solution, as do other β-pyrrole substituents.[8c]

The question remains, however, as to just how much steric crowding of the peripheral substituents is required to cause equilibrium between planar and nonplanar forms. And, in particular, can *meso*-substitution by planar aryl groups alone induce the appearance of nonplanar conformers? In this work, we obtained the resonance Raman spectra of (5,10,15,20-tetraphenylporphinato)nickel(II) [Ni(TPP)] in solution and in the solid state taken at 413.1- and 457.9-nm excitation wavelengths. The shapes of the lines ν_8 and ν_2 in solution are clearly asymmetric and composed of sublines belonging to planar and nonplanar conformers. This conclusion is based on earlier Raman studies[4,6,8] showing that nonplanar distortions decrease the frequencies for the line ν_2 and cause a red shift of the resonance positions in the Raman excitation profiles. This assignment is confirmed by the single-crystal Raman spectra of Ni(TPP), the X-ray crystal structure having been obtained recently for this purpose.[11] We also measured the temperature dependence of these lines at 297, 240, and 170 K. A reliable spectral analysis was employed yielding a decomposition of the line shapes into two sublines, giving the temperature-dependent ratios of the intensities of the sublines. Finally, either a two-state or three-state thermodynamic model is used to fit the intensity ratios of the sublines in the van't Hoff plot to determine the thermodynamic properties of the conformers. The main conclusion of this work is that Ni(TPP) in solution coexists in at least two distinctive conformers whose macrocycles differ in terms of nonplanarity as a result of the steric interaction between the phenyl groups and macrocycle.

Materials and Methods

Preparation. Ni(TPP) and Cu(TPP) were purchased from Porphyrin Products. The materials were purified by liquid chromatography using CS_2 as the mobile phase (column 1 × 10 cm^2; Silicia 32-63, 60 A, ICN Biomedicals). The CS_2 solvent was of HPLC grade. The homogeneity of the samples was monitored by thin-layer chromatography using Kieselgel with fluorescence indicator F254 (Merck). The preparation of the single crystals of Ni(TPP) is described elsewhere.[11]

Resonance Raman Spectroscopy. Solution and single-crystal Raman spectra at room temperature were obtained using dual-channel spectroscopy.[12] The single-crystal Raman spectra were recorded in the single-channel detection mode. Krypton and argon ion lasers (Coherent, Innova 20) provided excitation wavelengths in the B(Soret)- and Q-band regions of the absorption spectrum. A collection lens with a 30-cm focal length focused the laser beam onto the sample. The scattered light was collected in a 90° scattering geometry by using a camera objective (Canon lens 50 mm, 1:0.95; effective *f*/1.4) and imaged onto the entrance slit of the spectrometer (Spex 1401) equipped with a cooled photomultiplier (Hamamatsu, type R928P) and photon counting electronics (Tennelec, TC532 and TC593; LRS 133B and 123; Colorado Data System, 63B IAC System). A quartz cell was used for the solution spectra. The single crystals or crystalline powder were placed between two thin quartz slides and, in contrast to the solution spectra, the collection lens was defocused and the laser power at the solid sample was less than 20 mW to avoid strong local heating of the single crystal. After several scans, no sample decomposition was observed by checking the sample integrity of the single crystal under the microscope and by comparing the signals before and after the Raman measurements.

Raman measurements at different temperatures were carried out using a krypton ion laser (Coherent, Innova 90K).[8b] By using a cylindrical lens of 10-cm focal length, the linear polarized laser beam was focused onto the sample placed in a low-temperature cell consisting of a cylindrical quartz cuvette surrounded by a copper block. The cell was mounted onto the cold finger of a closed cycle cryostat (Leybold, ROK 10-300), and its temperature was regulated by a controller unit (Leybold, Variotemp HR1). The estimated errors for the temperature of the sample are ±5 K. The scattered light was collected in back-scattering geometry and imaged on the entrance slit of the spectrometer (Spex 1401) equipped with a cooled photomultiplier (RCA, type C31034-02) and photon-counting electronics (Ortec 9302, 9320).

Interference filters were used to suppress the interfering plasma lines of the gas ion lasers. Polarized spectra were measured by passing the scattered light through a Polaroid sheet oriented parallel or perpendicular to the scattering plane followed by a scrambler in front of the spectrometer entrance slit. The data obtained at different temperatures were stored in a computer which also controled the photon counter and the motor of the spectrometer.

For frequency calibration, the Raman spectra and the corresponding reference spectra were obtained simultaneously. At room temperature, the solution spectra of porphyrin sample and reference were obtained simultaneously by using a cylindrical rotating quartz cell consisting of two separate compartments (dual channel spectroscopy). Rotation of the Raman cell at 50 Hz prevented local heating of the sample even with incident laser powers at the sample as high as 100 mW. The frequency calibrations were carried out using benzene as reference; the observed peak positions of the benzene lines used were taken to be at 606.7, 992.2, and 1586.4/1606.2 cm^{-1}.[6d] On the other

hand, the frequency calibration of the solution spectra at different temperatures and the single-crystal spectra was carried out using suitable spectral lines of krypton and argon pencil lamps (Oriel). These spectral lines were also calibrated using the frequency positions of the benzene lines. These pencil lamps were mounted in front of the camera objective. The light from these lamps was directed onto the spectrometer slit for the short time that is necessary to record the spectral lines. The standard deviation in the observed frequency reading was ± 0.8 cm^{-1} for solution and ± 1.0 cm^{-1} for single-crystal spectra. Finally, all spectra were corrected for non-linearity of the spectrometer. The spectra shown in the figures are the unsmoothed sum of several scans; the specific conditions are described in the figure captions. The reproducibility of the spectra was verified by recording the spectra several times.

UV−Visible Absorption Spectroscopy. The absorption spectra were measured by using a Hewlett-Packard 8452 A diode array spectrophotometer and 10-mm quartz cell. The UV−vis spectra were used to check the sample integrity and to determine the porphyrin concentrations. The porphyrin concentrations for Ni(TPP) and Cu(TPP) in CS_2 solution were determined from the maximum absorbance of the B band using the extinction coefficients in CS_2 for Ni(TPP) and Cu(TPP). In the Raman experiment, the porphyrin concentrations were in the range from 0.1 to 0.5 mM.

Curve Fitting. The Raman lines were decomposed using Lorentzian lines convoluted with a triangularly shaped spectral slit function of the spectrometer.[13] A linear function was employed to fit the background intensity. The nonlinear least-squares curve fitting was carried out with the program PeakFit (Jandel Scientific). The spectral slit width $\tilde{s}$ of the slit function of the spectrometers (Czerny−Turner double monochromator) ranges from 2.4 to 5.6 cm^{-1} using 413.1-nm excitation wavelength and the 100- and 200-μm geometric slit widths S for the spectrometer.[8b] The experimentally determined slit function via spectral lines of krypton and argon pencil lamps can be described rather well with a triangular slit function for $S > 80$ μm and are fixed in the fitting procedure. The maximal deviations of the experimentally determined spectral slit widths to the calculated ones[8b] were less than 8%. The spectral slit width and the line width (or half-widths) of the Raman line are defined by the full width at half-maximum (fwhm). The intensity of a Raman (sub)line is given by the area. Also, the Raman line widths given in the text are all corrected for the spectrometer slit function and are therefore the true line widths. The fitted lines shown in the figures are the result of the convolution between the (true) Lorentzian line and the triangularly shaped spectral slit function.

Molecular Mechanics Calculations. The force field used for the classical molecular mechanics calculations has been described previously.[6a,e] It is based on the normal-mode analysis of Ni(OEP) and the DREIDING II force field. The energy minimization was carried out using POLYGRAPH software (Molecular Simulations, Inc.) and displayed on a Silicon Graphics workstation. In the calculation, the total energy is the sum of contributions from bond stretching, bending, torsions, inversions, electrostatic, and van der Waals energies.[14] In calculating the atomic electrostatic interactions for the charge distributions, the solvent dielectric constant was set to that of carbon disulfide (2.64). This force field is capable of accurately predicting the structures of various conformers and estimating their relative conformational energies. For example, Ni(OEP) is predicted to coexist in solution between a planar and nonplanar conformations as experimentally observed.[8]

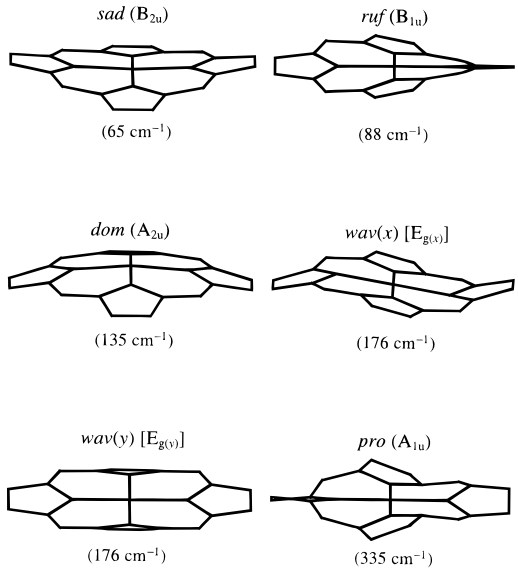

Figure 1. Illustrations of the lowest-frequency out-of-plane eigenvectors in coordinate space for each of the normal deformation $\hat{\mathbf{D}}_k^{oop}$ [*k*: *sad, ruf, dom, wav*(*x*), *wav*(*y*) and *pro*] used in describing the nonplanar distortions of the porphyrin macrocycle. Static displacements representing a 1-Å deformation along each lowest-frequency normal coordinate are shown (ref 2).

The conformational search for Ni(TPP) was carried out by varying the orientation of the substituents in each of the lowest-energy out-of-plane deformations;[2] that is, the *sad*, *ruf*, *dom*, or *wav* deformations were used as starting structures for the macrocycle for various substituent orientations before energy minimization. Then, the energy-minimized structures were also subjected to molecular dynamics simulations with the aim of finding additional energy minima.

Normal Structural Decomposition. The energy-minimized structures were analyzed using a new normal structural decomposition method for classifying and quantifying their out-of-plane and in-plane distortions.[2] The normal structural decomposition method characterizes the distortion in terms of equivalent displacements along the normal coordinates of the D_{4h}-symmetric porphyrin macrocycle (normal deformations). Theoretically, the out-of-plane (oop) and in-plane (ip) normal modes of each symmetry type (Γ_{oop} for 3 B_{2u}, 3 B_{1u}, 3 A_{2u}, 5 E_g, and 2 A_{1u}; Γ_{ip} for 6 B_{2g}, 6 B_{1g}, 11 E_u, 6 A_{1g}, and 5 A_{2g}) form a basis for characterizing the (internal) displacements of the 24 macrocyclic atoms.

As expected, it turns out that the predominate displacements arise from the lowest-frequency normal deformations (softest modes) of each symmetry type (minimal basis).[2] The minimal basis is illustrated in Figure 1 (out-of-plane) and 2 (in-plane).[15] The displacements along each of the minimal-basis deformations are listed in the tables as well as the mean deviations ($\bar{\delta}_{oop}$ and $\bar{\delta}_{ip}$) between the observed structure and the structure simulated by using the displacements along the deformations of the minimal basis. These mean deviations should be compared to the mean positional errors in X-ray crystallography for metalloporphyrins.[2,16]

Because of the high resolution of the X-ray crystal structures of metalloporphyrins, the small displacements for other normal coordinates than those of the minimal basis set can also be discerned.[2] Consequently, for a complete characterization of the energy-minimized structures, the total deformation along all of the modes of each symmetry type[2] D_{obs}^{Γ}, using the complete basis (21 out-of-plane and 45 in-plane normal deformations) are also given in the tables (complete basis). In

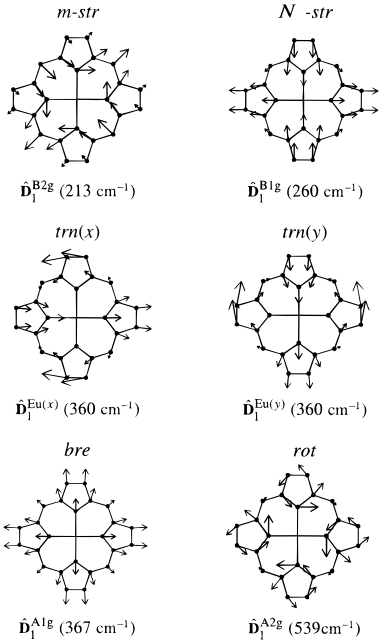

Figure 2. Illustrations of the lowest-frequency in-plane eigenvectors in coordinate space for each of the normal deformation $\hat{D}_k^{ip}$ [*k*: *meso-str*, *N-str*, *trn*(*x*), *trn*(*y*), *bre* and *rot*] used in describing the in-plane distortions of the porphyrin macrocycle. Static displacements representing a 1-Å deformation along each lowest-frequency normal coordinate are shown (ref 2).

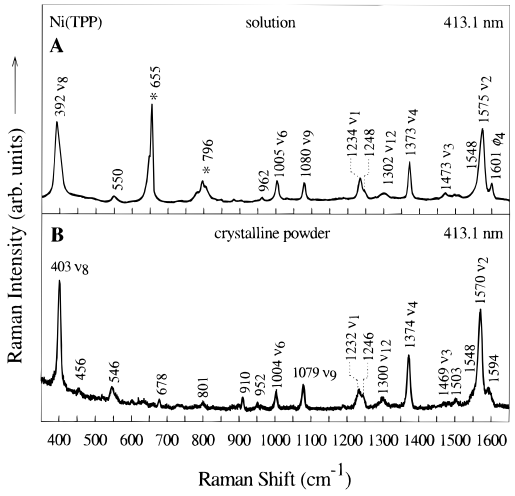

Figure 3. Overview resonance Raman spectra of Ni(TPP) in CS_2 solution (part A) and crystalline powder (part B) at room temperature. Conditions: 40 mW (solution), 10 mW (crystal); spectral resolution for 413.1-nm excitation is about 5 cm^{-1}, increment 0.5 cm^{-1}/s. The solvent lines are indicated with asterisks (*).

addition, the corresponding total out-of-plane and in-plane distortions, D_{oop} and D_{ip}, with respect to the copper reference macrocycle are useful quantities and are also listed for both the minimal and complete basis. A complete description of the normal structural decomposition method, the limits, and the application for synthetic and protein-bound porphyrins is given in previous papers.[1,2]

Results

Solution and Single-Crystal Raman Spectra at Room Temperature. Figure 3 displays an overview of the resonance Raman spectra of Ni(TPP) in CS_2 solution and in crystalline powder taken at room temperature. The assignment, labeling, and symmetry of the Raman lines are based on the recent normal-mode analysis.[17] The structure-sensitive skeletal modes enhanced at 413.1-nm excitation wavelength are ν_8, ν_4, ν_3, and ν_2.[6a,d,e,10,18] As can be seen from Figure 3, the peak frequencies of the lines ν_8, ν_3, and ν_2 are obviously different in solution and solid state; the frequency differences with respect to the solid-state spectra are -11, $+4$, and $+5$ cm^{-1}, respectively. (There are two lines in the region of ν_3 in the powder spectrum. ν_3 is assigned to the lower of these lines on the basis of a higher resolution spectrum [not shown] and the fact that ν_3 typically down shifts for nonplanar distortion.)[6d,8] Table 1 summarizes the frequency positions of the structure-sensitive lines of Ni(TPP) in solid state and in solution.

In the following, we focus our attention on the isolated skeletal modes that exhibit the largest frequency shifts upon changing the environment, that is, the structure-sensitive lines ν_8 and ν_2. Figure 4 (part A) displays an enlarged view of the lines ν_8 and ν_2 of Ni(TPP) in solution. These lines are broad ($\sim$16 cm^{-1}) and asymmetrically shaped. In contrast, the same lines in the single crystal (Figure 4, part C) are narrow ($\sim$8 cm^{-1}) and symmetric. Since Ni(TPP) in the single crystal exists only in one conformation,[11] the solution and single-crystal Raman spectra indicate that Ni(TPP) in solution may coexist in more than one conformer. To verify this, solution Raman measurements at different temperatures were carried out.

Raman Spectra at Different Temperatures and Line-Shape Analyses of ν_8 and ν_2. Raman spectra of Ni(TPP) in CS_2 were recorded at 297, 240, and 170 K. The lines ν_8 and ν_2 at temperature extremes are shown in Figure 4 (parts A and B). Obviously, the observed line shapes depend on temperature, with the high-frequency shoulder of the line ν_8 gaining intensity at low temperature as the most dramatic change.

The asymmetric lines ν_8 and ν_2 at different temperatures were decomposed into two sublines as shown in Figure 4. In the fitting procedure, the frequency positions, Lorentzian widths, and peak height of the high- (HF) and low-frequency (LF) sublines were used as free parameters. Analyzing the spectra at different temperatures reveals that each line, ν_8 or ν_2, is described well using only two sublines. Also, the spectroscopic parameters for the sublines of ν_8 are unequivocally determined and listed in Table 2 for the temperature extremes.

Figure 5 illustrates the temperature dependence of the lines ν_8 and ν_2 of Cu(TPP) at room and low temperatures. These lines are symmetric and narrow ($\sim$6 cm^{-1}) and are well fitted with single Lorentzian lines at different temperatures, indicating that Cu(TPP) in solution exists only in one conformation. The line widths and frequency positions of ν_8 and ν_2 at temperature extremes are also listed in Table 2.

For the sublines of ν_2 of Ni(TPP), the width of the sublines could not be reliably determined without any restrictions. For this purpose, the line width of ν_2 for Cu(TPP) at different temperatures was used, that is, the widths of the HF subline of ν_2 for Ni(TPP) were restricted to be almost the same values as found for Cu(TPP). Using this fitting procedure for Ni(TPP), we were able to obtain unique fitting parameters for the sublines of ν_2. The spectroscopic parameters ν_2 are listed in Table 2.

The curve fitting results show that the lines ν_8 and ν_2 at different temperatures can be described well by two sublines with temperature-dependent line widths. The widths of the LF and HF sublines become smaller as the temperature decreases. Moreover, the frequency positions for the sublines of ν_2 slightly increase with decreasing temperature. Interestingly, the LF sublines are narrow for ν_8 and broad for ν_2; this is reversed for the HF sublines (*i.e*, ν_8 is broad and ν_2 is narrow). A reversal is also noted for the intensity ratios I_{LF}/I_{HF}. Thus, we associate the broad and narrow sublines with different species, and we

TABLE 1: Frequencies (cm^{-1}) of the Structure-Sensitive Lines of Ni(OEP) and Ni(TPP) in the Single Crystals and in CS_2 Solution[a]

		Ni(TPP)			Ni(OEP)				
		crystal	solution		crystal			solution	
mode	sym	tetragonal	planar	nonplanar	triclinic **A**[b]	triclinic **B**[b]	tetragonal	planar	nonplanar
ν_8	A_{1g}	403[c]	392[c]	400[c]	342[d]	354[d]	345[d]	340/361[e,f]	
ν_4	A_{1g}	1374[c]	1373[c,g]		1382[h]	1383[h]	1382[h]	1383[g,f]	
ν_3	A_{1g}	1469[c]	1473[c,g]		1522[h]	1526[h]	1513[h]	1521[f]	1518[f]
ν_{11}	B_{1g}	1504[i]	1512[j]	1506[j]	1580[h]	1580[h]	1570[h]	1578[f]	1575[f]
ν_{19}	A_{2g}	1550[i]	1557[j]	1547[j]	1606[d]	1608[d]	1589[k]	1604[l]	1597[l]
ν_2	A_{1g}	1570[c]	1578[c]	1572[c]	1608[h]	1609[h]	1595[h]	1600[m]	
ν_{10}	B_{1g}	1594[i]	1604[j]	1598[j]	1661[h]	1663[h]	1640[h]	1659[l]	1652[l]

[a] Estimated errors for the frequencies are about ± 1.0 cm^{-1}. [b] Absolute frequencies of the lines are systematically higher than those in ref 9. Frequency differences between the triclinic **A** and **B** forms are due to intermolecular stacking interactions in the **B** form (ref 9). [c] This work. [d] Reference 9. [e] Line appears as a doublet due to different ethyl orientations (ref 21). [f] Reference 19. [g] Sublines could not be reliably resolved or the composite line appears as a single line; the observed peak position is given. [h] Reference 20. [i] Frequency positions in KCl pellet (ref 17). [j] Reference 22a. [k] Reference 10. [l] Reference 8b. [m] Line shape is clearly asymmetric, but the sublines could not be reliably resolved due to spectral crowding (ref 8b).

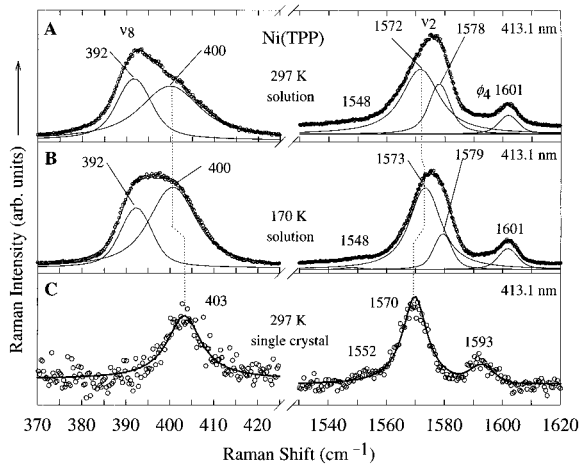

Figure 4. Resonance Raman spectra for the structure-sensitive lines ν_8 and ν_2 of Ni(TPP) in CS_2 solution at room (part A) and low (part B) temperature and in the single crystal at room temperature (part C). The solid lines are the results of the decomposition of the asymmetric line shapes into two sublines (fitting procedure is described in text). Conditions: 20 mW (solution), 10 mW (crystal); spectral resolution for 413.1-nm excitation is about 5 cm^{-1}; increment 0.3 cm^{-1}/s (solution), increment 0.5 cm^{-1}/s (crystal).

TABLE 2: Spectroscopic Parameters (Frequency $\tilde{\nu}$ and Half-Width Γ in cm^{-1}) for the (Sub)Lines of ν_8 and ν_2 for Ni(TPP) and Cu(TPP) in CS_2 Solution at Room (297 K) and Low (170 K) Temperatures[a]

		ν_8				ν_2[b]			
		planar		nonplanar		planar		nonplanar	
porphyrin	parameter	297	170	297	170	297	170	297	170
Ni(TPP)	$\tilde{\nu}$	392	392	400	400	1578	1579	1572	1573
	Γ	6	5	15	11	6	4	14	11
Cu(TPP)	$\tilde{\nu}$	392	393			1563	1565		
	Γ	5	4			7	5		

[a] Error estimates are 15% for the line widths and ± 1 cm^{-1} for the frequency positions. [b] Line widths of the HF sublines of Ni(TPP) in solution are restricted to be almost the same as the line width of Cu(TPP) due to ambiguity in the curve-fitting procedure (see text).

plotted the intensity ratio I_{broad}/I_{narrow} *versus* $1/T$ in Figure 6. Straight lines with almost equal slopes are found for both lines in the van't Hoff plots.

Raman Line Shape at Different Excitation Wavelengths. Similar behavior is also found in the selective enhancement of the sublines of ν_8 and ν_2 using different excitation wavelengths. Figure 7 displays the shape of the lines ν_8 and ν_2 at different excitation wavelengths for Ni(TPP) in solution and in the single crystal. The wavelengths selected are on the blue and red side of the B band in the UV−visible absorption spectra (see inset in Figure 7). For the single crystal, no significant changes are observed in the line shape, but the Raman lines apparently change their shape in solution. When using excitation wavelengths located on the red side of the B band, the HF subline of ν_8 and the LF subline of ν_2 gain intensity. In other words, the broad lines representing one conformer are selectively enhanced on the red side of the B band. In addition, the broad and narrow sublines of ν_8 and ν_2 have different resonance positions in their Raman excitation profiles, indicating that

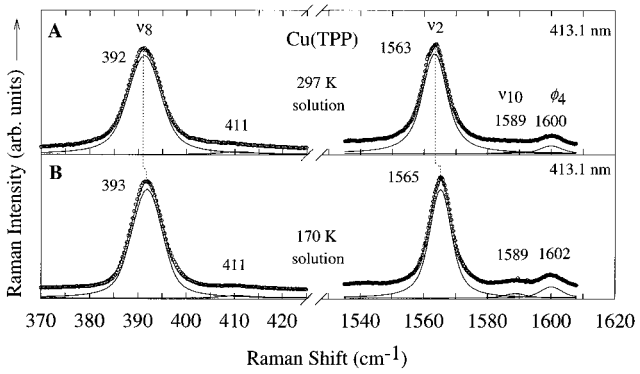

Figure 5. Resonance Raman spectra for the structure-sensitive lines ν_8 and ν_2 of Cu(TPP) in CS_2 solution at room (part A) and low temperature (part B). Conditions: 20 mW, spectral slit width for 413.1-nm excitation is about 5.1 cm^{-1}, increment 0.3 cm^{-1}/s.

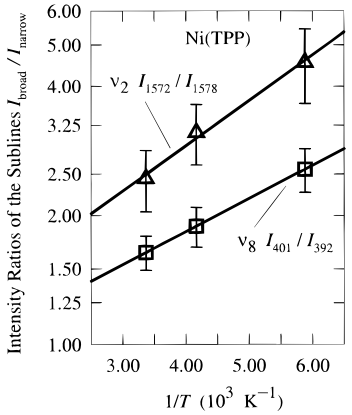

Figure 6. van't Hoff plots of the intensity ratios of the sublines of ν_8 and ν_2 for Ni(TPP). The solid lines are the calculated values according to the two-state [eq 1] and three-state models [eq 3]. Fitting parameters are given in Table 5. The bars illustrate the maximum errors in determining the intensity ratios.

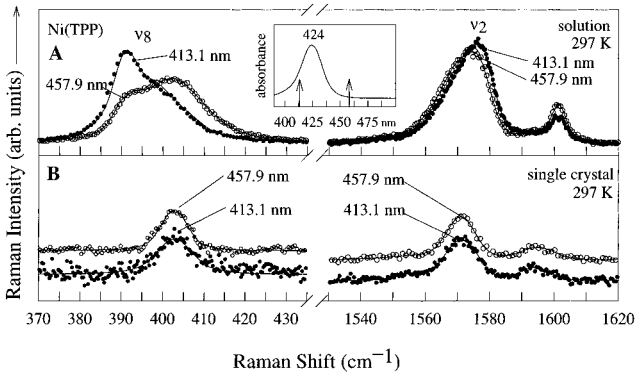

Figure 7. Resonance Raman spectra at different excitation wavelengths for the structure-sensitive lines ν_8 and ν_2 of Ni(TPP) in CS_2 solution (part A) and in the single crystal (part B) at room temperature. The spectra were obtained by exciting on the red and blue sides of the B band of the UV−vis spectrum (arrows in the inset show the positions of the excitation wavelengths). Spectral resolution for 413.1-nm excitation on 3 cm^{-1} (solution) and 5 cm^{-1} (crystal). For 457.9-nm excitation, the resolution is 2 cm^{-1} (solution) and 4 cm^{-1} (crystal). Conditions: 80 mW (solution), 20 mW (crystal), increment 0.3 cm^{-1}/s (solution), increment 0.5 cm^{-1}/s (crystal).

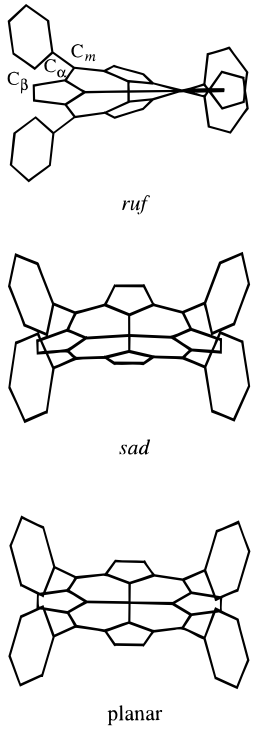

Figure 8. The three energy-minimized conformers predicted for Ni(TPP). The *ruf* conformation is the lowest-energy conformer; the *sad* and planar conformations have almost the same energies. For clarity, the hydrogen atoms are not shown. The carbon atom labeling is also shown.

the absorption bands of the two conformers are shifted with respect to each other.

Molecular Mechanics Calculations. All stable conformers of Ni(TPP) were found by energy minimization starting from initial structures having all possible combinations of the orientations of the phenyl groups and out-of-plane macrocyclic structures. There are three stable energy-minimized conformers, the *ruf*, *sad*, and planar conformations illustrated in Figure 8. The calculated energies for each of the predicted conformers are summarized in Table 3. It was found that the *ruf* conformer is the lowest-energy structure; the *sad* and planar conformers have almost the same energy, which is about 7 kJ mol^{-1} higher than the *ruf* conformer.

Normal Structural Decomposition of the Energy-Minimized and X-ray Crystal Structures. Table 4 lists the displacements along the out-of-plane and in-plane normal deformations for the energy-minimized structures obtained using the minimal and complete basis. As expected, the structures are simulated well using only the minimal basis. The two energy-minimized nonplanar structures are purely ruffled (1.475 Å) and purely saddled (−1.082 Å) and exhibit an in-plane A_{1g} contraction (*bre* deformation) with respect to the copper reference macrocycle. In all cases, the negative *bre* deformation is due to both the small nickel ion for the porphinato core and the nonplanar distortion. For the planar conformer, very small amounts of *sad* and *ruf* deformations are found. The total observed out-of-plane distortions are 1.478, 1.082, and 0.022 Å for the *ruf*, *sad*, and almost planar conformers, respectively.

Besides the different macrocyclic conformations of the energy-minimized structures for Ni(TPP), the three conformers also differ in the phenyl orientations. For the *ruf* and planar conformations, the phenyl groups are all perpendicular with respect to the $C_\alpha C_m C_\alpha$ plane characterized in Table 4 as *PPPP* orientation. On the other hand, the phenyl groups in the *sad* conformer are alternatively tilted left (*L*) or right (*R*) with respect to the $C_\alpha C_m C_\alpha$ plane. The average tilting angles are the same for all phenyl groups and is about 84°. This arrangement in the *sad* conformation is designated in Table 4 as *LRLR* orientation.

For comparison, Table 4 also lists the displacements for the X-ray crystal structure for Ni(TPP).[11] This X-ray crystal structure was obtained from the same single crystal that was used for the Raman measurements in this work. From Table 4, in the X-ray crystal structure Ni(TPP) is predominately ruffled (1.296 Å) and saddled (−0.237 Å). Furthermore, apart from the expected *bre* in-plane deformation, a small but significant amount of *rot* deformation is observed in the X-ray crystal structure, a common feature of other X-ray crystal structures of metallotetraphenylporphyrins.[11] The total observed out-of-plane and in-plane distortions are 1.321 and 0.322 Å, respectively. A detailed description and analysis of the X-ray crystal structures of Ni(TPP) and other metallotetraphenylporphyrins are given in a separate paper.[11]

Discussion

Raman studies of substituted metalloporphyrins[6] in crystalline forms[9,10] and in solution[4,8] have shown that nonplanar distortions of the macrocycle of the *ruf* and *sad* deformation types cause a downshift of the frequencies of the Raman lines ν_3, ν_{11}, ν_2, ν_{19}, and ν_{10}. The downshifts in frequencies parallel the red shift of the UV−visible absorption bands resulting from nonplanar distortion. Table 1 lists the frequencies of the lines for the three types of crystals of Ni(OEP)—the two planar (triclinic A and B forms) and one strongly nonplanar form (tetragonal *C*)—illustrating the downshifts of the structure-sensitive lines. Raman studies[8b] of Ni(OEP) in solution show that the Raman lines ν_3, ν_{11}, ν_{19} and ν_{10} can be decomposed into two sublines, and the subline attributed to the nonplanar conformer is generally broader than the subline of the planar conformer. The frequencies of the sublines of the nonplanar and planar conformers of Ni(OEP) in solution are also listed in Table 1 for comparison with the Raman data for Ni(TPP).

Assignment of the Broad and the Narrow Sublines of ν_8 and ν_2 of Ni(TPP) to Nonplanar and Planar Conformers. The decomposition of the Raman lines ν_8 and ν_2 of Ni(TPP) in CS_2 solution reveals two sublines with different widths. Further, the relative intensity of the sublines depends on temperature

TABLE 3: Energies (kJ mol^{-1}) for the Energy-Minimized Stable Conformers of Ni(TPP)

conformer	relative[a]	total	bonds	angles	torsions	inversions	van der Waals	electrostatic
ruf	0.00	756.62	40.02	295.53	198.83	2.73	251.79	−32.20
sad	7.10	763.72	49.15	302.48	173.23	1.03	269.83	−32.00
planar	7.46	764.08	52.00	302.29	167.48	0.00	274.25	−31.94

[a] Energy relative to the lowest-energy conformer.

TABLE 4: Out-of-Plane and in-Plane Displacements (Å) for the Minimal (Italics) and Complete Normal Coordinate Basis (Bold) for the X-ray Crystal and Energy-Minimized Structures of Ni(TPP). Total Deformation of Each Symmetry type[2] Is Found Using the Complete Basis[a]

		out-of-plane displacements								in-plane displacements							
Ni(TPP) conformer[b]	orientation[c]	D_{oop}[d]	$\bar{\delta}_{oop}$[d]	*sad* (B_{2u})	*ruf* (B_{1u})	*dom* (A_{2u})	*wav*(*x*) ($E_g(x)$)	*wav*(*x*) ($E_g(y)$)	*pro* (A_{1u})	D_{ip}[d]	$\bar{\delta}_{ip}$[d]	*m-str* (B_{2g})	*N-str* (B_{1g})	*trn*(*x*) ($E_u(x)$)	*trn*(*x*) ($E_u(y)$)	*bre* (A_{1g})	*rot* (A_{2g})
energy-minimized																	
ruf, [$D_{2d}(C_2')$]	*PPPP*	*1.475*	*0.015*	*0*	*1.475*	*0*	*0*	*0*	*0*	*0.358*	*0.022*	*0*	*0*	*0*	*0*	*-0.358*	*0*
		1.478		**0**	**1.478**	**0**	**0**	**0**	**0**	**0.380**		**0**	**0**	**0**	**0**	**0.380**	**0**
sad [$D_{2d}(C_2'')$]	*LRLR*	*1.082*	*0.005*	*−1.082*	*0*	*0*	*0*	*0*	*0*	*0.202*	*0.021*	*0*	*0*	*0*	*0*	*−0.202*	*0*
		1.082		**1.082**	**0**	**0**	**0**	**0**	**0**	**0.231**		**0**	**0**	**0**	**0**	**0.231**	**0**
planar (D_{4h})	*PPPP*	*0.022*	*0.000*	*−0.015*	*0.016*	*0*	*0*	*0*	*0*	*0.118*	*0.019*	*0*	*0*	*0*	*0*	*−0.118*	*0*
		0.022		**0.015**	**0.016**	**0**	**0**	**0**	**0**	**0.156**		**0**	**0**	**0**	**0**	**0.156**	**0**
X-ray crystal																	
ruf + *sad* (S_4)	*LRLR*	*1.317*	*0.017*	*−0.237*	*1.296*	*0*	*0*	*0*	*0*	*0.312*	*0.015*	*0*	*0*	*0*	*0*	*−0.311*	*−0.027*
		1.321		**0.256**	**1.296**	**0**	**0**	**0**	**0**	**0.322**	**0.000**	**0**	**0**	**0.001**	**0.001**	**0.319**	**0.048**

[a] Displacements were obtained by orienting the macrocycle consistently in such a way that the displacements are negative for *sad* and/or positive for *ruf* deformations. [b] Point group symmetry is based on both the substituent orientation and the macrocyclic conformation. The 2-fold symmetry axes C_2' and C_2'' refer to the D_{4h} point group. [c] Approximate dihedral angle between the phenyl and the $C_\alpha C_m C_\alpha$ plane is 90° for the *PPPP* orientation. For the *LRLR* orientations in the energy-minimized and X-ray crystal structures, the angles are 84° and 78°, respectively. [d] Total simulated distortions D_{oop} and D_{ip} (Å) and the mean deviations, $\bar{\delta}_{oop}$ and $\bar{\delta}_{ip}$ (Å) for the minimal basis set are given; the simulation is exact for the complete basis.

and excitation wavelength. The HF subline of ν_8 and the LF subline of ν_2 are broad, whereas the LF subline of ν_8 and the HF subline of ν_2 are narrow. Figure 6 displays the van't Hoff plots of the intensity ratios I_{broad}/I_{narrow} for the sublines of ν_8 and ν_2. On the basis of temperature dependence and line widths, we assign the broad sublines to one type of conformer and the narrow sublines to another.

In analogy with Ni(OEP), the broad LF subline of ν_2 for Ni(TPP) arises from a nonplanar conformer, whereas the narrow HF subline results from a more planar conformer. This accounts also for the red shift of the Raman excitation profile of the LF subline of ν_2 with respect to the profile of the HF subline, since a red shift in the absorption bands of the nonplanar conformer is expected. (In the curve-fitting procedure, it is therefore reasonable to assume that the width of the HF subline of ν_2 at different temperatures is similar to the width of the presumably planar conformer of Cu(TPP) in solution at the same temperatures.[23])

In general, there is no simple relationship between the frequency of ν_8 and the degree of nonplanarity,[6d,] but it is known that the shape of ν_8 is sensitive to structural heterogeneity.[6d,e21] On the basis of the broadness of the HF subline of ν_8 and its considerable enhancement using an excitation wavelength located on the red side of the B band, we infer that the HF subline of ν_8 arises from a nonplanar conformer and the LF subline of ν_8 comes from a more planar conformer.

An alternative interpretation for the asymmetric shape of the lines ν_8 and ν_2 for Ni(TPP) in solution might be spectral crowding, that is, other lines underlying ν_8 and ν_2 cause the asymmetry. However, this seems unlikely because the asymmetric shapes of the lines ν_8 and ν_2 for Ni(TPP) in solution are still present after deuteration at different positions.[24] Moreover, as can be seen from Figure 4 (part C), the lines ν_8 and ν_2 in the single-crystal Raman spectra are symmetric and relatively narrow, as expected for the single crystal of Ni(TPP) which contains only one conformer. Thus, spectral crowding as an alternative interpretation for the asymmetric line shapes is rather unlikely. Moreover, spectral crowding cannot easily explain the systematic change of the intensity ratios of the sublines with temperature.

Two-State Thermodynamic Model. Ni(TPP) in solution coexists in at least two conformers whose macrocycles differ with respect to the degree of nonplanarity. The simplest thermodynamic model for interpreting the temperature dependence of the intensity ratios consists of two states, a planar (pl) and a nonplanar (npl) conformer. Following the analysis of the sublines for Ni(OEP) in a recent paper,[8b] the intensity ratio as a function of temperature can be expressed as follows:

$$\frac{I_{npl}}{I_{pl}} = \frac{I_{broad}}{I_{narrow}} = \frac{\sigma_{npl}}{\sigma_{pl}}\frac{n_{npl}}{n_{pl}} = \frac{\sigma_{npl}}{\sigma_{pl}}\exp\left(\frac{\Delta G_{pl,npl}}{RT}\right) \qquad (1)$$

The Raman cross sections of the two conformers are σ_{npl} and σ_{pl}, the occupation numbers of the nonplanar and planar states are n_{npl} and n_{npl}, T is the absolute temperature, and R is the universal gas constant. $\Delta G_{pl,npl}$ is the Gibbs free energy difference between the two states defined by the Gibbs−Helmholtz equation, $\Delta G_{pl,npl} = \Delta H_{pl,npl} - T\Delta S_{pl,npl}$. The thermodynamic parameters $\Delta H_{pl,npl}$ and $\Delta S_{pl,npl}$ are the enthalpic and entropic differences between the two states.

The thermodynamic parameters of the two-state model, which were determined from the fits to the data in Figure 6 (solid lines), are listed in Table 5 and are similar for the lines ν_8 and ν_2. The entropic difference is calculated by assuming that the Raman cross sections for the two conformers are the same. However, this assumption is likely incorrect because the excitation profiles for the planar and nonplanar forms are shifted with respect to each other and, therefore, the Raman cross sections for the two forms depend on the excitation wavelength. In our case, the 413.1-nm excitation selectively enhances the planar conformer (see Figure 7). In addition, the difference in the degeneracy factors between the planar and nonplanar form complicates the interpretation of the entropy (*vide infra*); thus, the entropic value is unreliable.

TABLE 5: Thermodynamic Parameters (ΔH in kJ mol^{-1} and ΔS in kJ mol^{-1}) for the Two-State [Equation 1] and Three-State [Equation 3] Models Derived from the van't Hoff Plots of the Intensity Ratios of the Sublines of ν_8 and ν_2 for Ni(TPP) in CS_2 Solution

model	parameters	ν_8	ν_2
two-state[a]	$\Delta H_{pl,npl}$[b]	1.5 ± 1.0	2.0 ± 1.0
	$\Delta S_{pl,npl}$[c]	0.9 ± 4	-1.0 ± 4
three-state[d,e]	$\Delta H_{sad,ruf}$, $\Delta H_{pl,ruf}$[f]	2.0 ± 1.0	2.5 ± 1.3
	$(\sigma_{pl}/\sigma_{npl})$[g]	3.9 ± 1.5	2.9 ± 1.5

[a] Assumes one almost planar (pl) and one nonplanar (npl) structure, *ruf* or *sad* conformation. [b] Enthalpic differences are respect to the nonplanar conformer. [c] Because the Raman cross sections for the nonplanar and planar conformers are assumed to be the same, the entropic difference is physically unreasonable. [d] On the basis of the molecular mechanics calculations, the model assumes a *ruf*, *sad*, and planar conformation. [e] The degeneracy factors g are set to be 1 and 2 for the planar and nonplanar forms, respectively. [f] Enthalpic differences are with respect to the *ruf* conformer. Energies are set to be the same for the *sad* and planar forms consistent with the molecular mechanics calculations. [g] Ratio of the Raman cross section at 413.1-nm excitation wavelength.

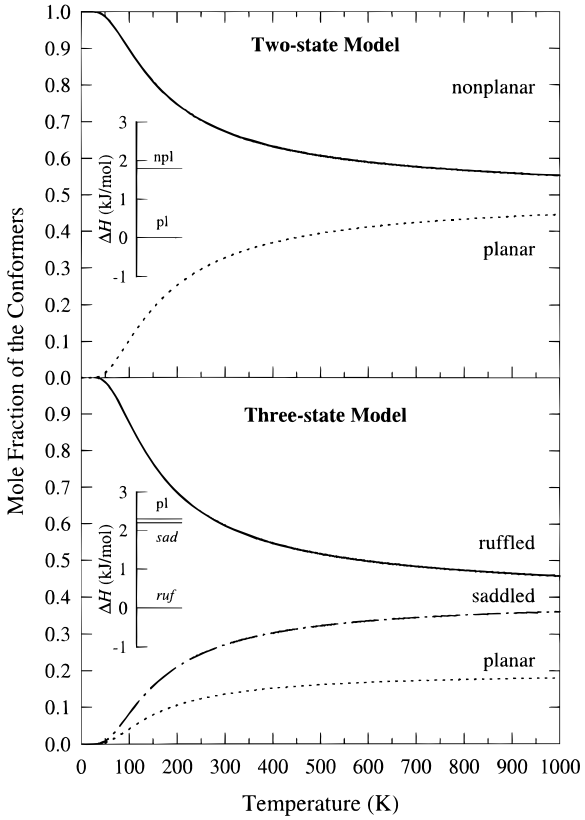

Figure 9. Mole fraction of the conformers determined according to the two-state and three-state model using eqs 1 and 3, respectively. In the calculation, the average enthalpic energies for the lines ν_8 and ν_2 are used, that is, 1.8 and 2.3 kJ mol^{-1} for the two-state and three-state model, respectively. In calculating the mole fractions in the two-state model, the Raman cross sections for the nonplanar and planar conformers are assumed to be the same and the entropic difference is zero. For the three-state model, the degeneracy factors are set to $g_{npl} = g_{ruf} = g_{sad} = 2$ and $g_{pl} = 1$.

In summary, the two-state thermodynamic model accounts for the temperature dependence of the intensity ratios and the change in the shape of the Raman lines upon changing the excitation wavelengths. The two sublines of ν_8 and ν_2 result from conformers with planar and nonplanar macrocycles. The nonplanar conformer in CS_2 solution is energetically favored by about 1.8 kJ mol^{-1}. Figure 9 (part A) illustrates the mole fractions of the conformers according to the two-state model.

Three-State Thermodynamic Model. Another possible interpretation for the temperature dependence of the intensity ratios is suggested by the molecular mechanic calculations. This model involves three conformational states and associates these conformers with specific structures, two nonplanar (*sad* and *ruf*) and one planar form. Since the degree of nonplanarity for the *ruf* and *sad* energy-minimized structures is similar (see Table 4), their corresponding structure-sensitive lines probably coincidentally appear almost at the same frequencies and give rise to the composite broad nonplanar sublines. On the other hand, the planar energy-minimized structure emerges in the Raman spectra as a single narrow subline. In this case, the intensity ratio as a function of temperature can be expressed as follows:

$$\frac{I_{npl}}{I_{pl}} = \frac{I_{ruf} + I_{sad}}{I_{pl}} = \frac{\sigma_{ruf}\, n_{ruf} + \sigma_{sad}\, n_{sad}}{\sigma_{pl}\, n_{npl}} = \frac{\sigma_{ruf}}{\sigma_{pl}} \exp\left(\frac{\Delta G_{pl,ruf}}{RT}\right)\left[1 + \frac{\sigma_{sad}}{\sigma_{ruf}} \exp\left(-\frac{\Delta G_{sad,ruf}}{RT}\right)\right] \quad (2)$$

Because there are too many free parameters involved, we must make some additional assumptions in this model. It is reasonable to assume that the entropic differences arise only from the different degeneracy factors g (*i.e.*, the number of the energetically identical nondistinguishable states). We then obtain the following equation for the intensity ratio as a function of temperature:

$$\frac{I_{npl}}{I_{pl}} = \frac{\sigma_{ruf}}{\sigma_{pl}} \frac{g_{ruf}}{g_{pl}} \exp\left(\frac{\Delta H_{pl,ruf}}{RT}\right)\left[1 + \frac{\sigma_{sad}}{\sigma_{ruf}} \frac{g_{sad}}{g_{ruf}} \exp\left(-\frac{\Delta H_{sad,ruf}}{RT}\right)\right] \quad (3)$$

The degeneracy factors are 2 for the nonplanar conformers and 1 for the planar conformer. This is because the opposite pyrrole planes for the *ruf* conformer can be twisted counterclockwise or clockwise with respect to an axis through the nitrogen atoms (see Figure 8). The same reasoning is true for the *sad* conformer (pyrrole planes can be tilted above or below the mean plane of the macrocycle). Moreover, it is also reasonable to assume that the Raman cross sections are nearly the same for the two nonplanar conformers ($\sigma_{ruf} = \sigma_{sad}$). Finally, in accord with the molecular mechanics calculations, the enthalpic differences are set equal for the *sad* and planar forms ($\Delta H_{sad,ruf} = \Delta H_{pl,ruf}$). In fitting the intensity ratio, the only free parameters in this equation are therefore the enthalpic difference between the nonplanar and planar conformers and the ratio σ_{pl}/σ_{npl} of the Raman cross sections.

The thermodynamic parameters of the three-state model, which were determined from the fits to the data in Figure 6 (solid lines), are listed in Table 5 and are similar for the lines ν_8 and ν_2. The enthalpic difference of the *sad* and planar conformers with respect to the *ruf* conformer is about 2.3 kJ mol^{-1} that deviates by a factor of about four from the calculated value (see Table 3). Such an error is certainly possible given that the relative energies obtained from molecular mechanics calculations are in the range of only several kJ mol^{-1}. Also, the detailed solvent−porphyrin interactions, which can also have a contribution to the enthalpic difference, are not included in the molecular mechanics calculations. The Raman cross section for the planar conformation is about 3 times larger than that of the nonplanar conformers. Moreover, the large difference in the Raman cross section between the nonplanar and planar conformers of Ni(TPP) is expected since the excitation wavelengths used in the temperature measurements selectively enhance the planar conformation.

Taken together, the three-state model accounts for the temperature dependence of the intensity ratios of the sublines and is consistent with the predictions of the molecular mechanics calculations. The *ruf* conformer is stabilized by about 2.3 kJ mol^{-1} with respect to the energetically equal *sad* and planar conformers. The entropic part arises from the different degeneracy factors for the planar and nonplanar structures. Figure 9 (part B) illustrates the mole fractions of the conformers according to the three-state model.

Types of Nonplanar Conformers of Ni(TPP) in Solution for the Two-State and Three-State Model. In the single crystal, Ni(TPP) is strongly nonplanar (total distortion = 1.321 Å) and is mainly of a *ruf* deformation type (see Table 4; the $C_\alpha N-NC_\alpha$ dihedral angle is about 30°).[11] Our assignment of sublines of ν_8 and ν_2 to nonplanar conformers is consistent with the frequencies of these lines in the single-crystal Raman data, (*i.e.*, the frequencies of the sublines resulting from the nonplanar forms in solution almost match the Raman frequencies of the single crystal). This may indicate that the macrocycle of the nonplanar form in solution is predominantly ruffled. If so, the magnitude of the *ruf* deformation in solution must be similar to that observed for the X-ray crystal structure.

A recent study[11] suggests that the small *sad* contribution evident in the X-ray crystal structure for many metallotetraphenylporphyrins is probably caused by the crystal packing arrangement, specifically its effect on the tilting of the phenyl planes. Thus, the *sad* deformation (−0.237 Å) in the X-ray crystal structure of Ni(TPP) is mainly due to the *LRLR* phenyl orientation.[11] The *ruf* conformer of Ni(TPP) in solution is expected to be in the energetically favored *PPPP* phenyl orientation as found in the molecular mechanics calculations. This implies that the nonplanar conformer of Ni(TPP) is probably *purely* of the *ruf* deformation type.

It remains possible however that the nonplanar conformer is simultaneously both ruffled and saddled as observed in the X-ray crystal structure of Ni(TPP). The resulting point group symmetry is then S_4, whereas the pure *ruf* or *sad* deformations have D_{2d} symmetry. The symmetry of Ni(TPP) in solution can be determined by Raman dispersion spectroscopy.[5c,26] More specifically, for S_4 symmetry we expect dispersion of the depolarization ratio for the A_{1g} HF subline of ν_8 and LF subline of ν_2 ($\rho \geq 1/8$), the lines attributed to the nonplanar forms; this question will be addressed in a future paper.[22b]

Disregarding the calculated relative energies for the *ruf* and *sad* conformers in the molecular mechanics calculations, it is also quite possible that the nonplanar form of Ni(TPP) in solution may exist in the pure *sad* deformation. The structure-sensitive lines in solution would probably appear at almost the same frequencies as for the *ruf* deformation.[6a] An alternative notion consistent with the three-state model is that both *sad* and *ruf* conformers coexist in solution. Both *sad* and *ruf* deformations cause similar downshifts of the structure-sensitive lines[6a] since the calculated degree of nonplanarity for the *sad* conformer (1.082 Å) is similar to that of the *ruf* conformer (1.475 Å). Spectroscopically, the frequencies of the two types of nonplanar conformers would not be distinguishable because of the near degeneracy of their frequencies. Other vibrational lines may allow one to conclusively determine the types of distortion that occurs in solution.

In summary, Ni(TPP) in solution coexists in at least two distinctive conformers whose macrocycles differ in terms of nonplanarity. This accounts for the asymmetric shapes of the structure-sensitive Raman lines ν_8 and ν_2 and their change with temperature and excitation wavelengths. Two thermodynamic models, a two-state and a three-state model, are proposed to fit the van't Hoff plots of the intensity ratios of the sublines, showing that the nonplanar conformer is energetically favored by about 2.0 kJ mol^{-1}. The nonplanar conformer in the two-state model is most likely either a purely *ruf* conformer or a conformer composed of a mixture of both *sad* and *ruf* deformations. Although there is no direct evidence for the additional *sad* conformer proposed in the three-state model, the possibility finds support from the molecular mechanics calculations. The most stable conformer of Ni(TPP) probably consists of mainly a *ruf* deformation because displacement along the *ruf* coordinate for metallotetraphenylporphyrins requires almost no energy as long as the *ruf* deformation is less than or equal to 1 Å.[11]

Acknowledgment. Sandia is a multiprogram laboratory operated by Sandia Corporation, a Lockheed Martin Company, for the United State Department of Energy under Contract DE-AC04-94DP85000.

References and Notes

(1) Jentzen, W.; Ma, J.-G.; Shelnutt, J. A. *Biophys. J.* **1997**. Submitted for publication.

(2) Jentzen, W.; Song, X.-Z.; Shelnutt, J. A. *J. Phys. Chem. B* **1997**, *101*, 1684.

(3) (a) Lesk, A. M.; Chotia, C. H. *Philos. Trans. R. Soc. London* **1986**, *A317*, 345. (b) Lesk, A. M.; Levitt, M.; Chotia, C. H. *Protein Eng.* **1986**, *1*, 77. (c) Sweet, R. M. *Biopolymers* **1986**, *25*, 1565. (d) Hasemann, C. A.; Kurumbail, R. G.; Boddupalli, S. S.; Peterson, J. A.; Deisenhofer, J. *Structure* **1995**, *3*, 41.

(4) Anderson, K. K.; Hobbs, J. D.; Luo, L.; Stanley, K. D.; Quirke, J. M. E.; Shelnutt J. A. *J. Am. Chem. Soc.* **1993**, *115*, 12346.

(5) (a) Shelnutt, J. A.; Rousseau, D. L.; Dethmers, J. K.; Margoliash, E. *Biochemistry* **1981**, *20*, 6485. (b) Morikis, D.; Champion, P. M.; Springer, B. A.; Sligar, S. G. *Biochemistry* **1989**, *28*, 4791. (c) Schweitzer-Stenner, R. *Q. Rev. Biophys.* **1989**, *22*, 381. (d) Abdachi, S.; Nagano, S.; Ishimori, K.; Watanabe, Y.; Morishima, I.; Egawa, T.; Kitagawa, T.; Makino, R. *Biochemistry* **1993**, *32*, 241. (e) Mitchell, D. M.; Ådelroth, P.; Hosler, J. P.; Fetter, J. R.; Brzezinski, P.; Pressler, M. A.; Aasa, R.; Malmström, B. G.; Alben, J. O.; Babcock, G. T.; Gennis, R. B.; Ferguson-Miller, S. *Biochemistry* **1996**, *35*, 824.

(6) (a) Shelnutt, J. A.; Medforth, C. J.; Berber, M. D.; Barkigia, K. M.; Smith, K. M. *J. Am. Chem. Soc.* **1991**, *113*, 4077. (b) Shelnutt, J. A.; Majumder, S. A.; Sparks, L. D.; Hobbs, J. D.; Medforth, C. J.; Senge, M. O.; Smith, K.M.; Miura, M.; Quirke, J. M. E. *J. Raman Spectrosc.* **1992**, *23*, 523. (c) Hobbs, J. D.; Majumder, S. A.; Luo, L.; Sickelsmith, G. A.; Quirke, J. M.E.; Medforth, C. J.; Smith, K. M.; Shelnutt J. A. *J. Am. Chem. Soc.* **1994**, *116*, 3261. (d) Jentzen, W.; Simpson, M. C.; Hobbs, J. D.; Song, X.-Z.; Ema, T.; Nelson, N. Y.; Medforth, C. J.; Smith, K. M.; Veyrat, M.; Mazzanti, M.; Ramasseul, R.; Marchon, J.-C.; Takeuchi, T.; Goddard, W. A., III; Shelnutt, J. A. *J. Am. Chem. Soc.* **1995**, *117*, 11085. (e) Song, X.-Z.; Jentzen, W.; Jia, S.-L.; Jaquinod, L.; Nurco, D. J.; Medforth, C. J.; Smith, K. M.; Shelnutt, J. A. *J. Am. Chem. Soc.* **1996**, *118*, 12975.

(7) (a) Jentzen, W.; Shang, M.; Scheidt, W. R.; Song, X.-Z.; Jia, S; Shelnutt, J. A. In preparation. (b) Jentzen, W.; Turowska-Tyrk, I.; Scheidt, W. R.; Shelnutt, J. A. *Inorg. Chem.* **1996**, *35*, 3559.

(8) (a) Alden, R. G.; Crawford, B. A.; Doolen, R.; Ondrias, M. R.; Shelnutt, J. A. *J. Am. Chem. Soc.* **1989**, *111*, 2070. (b) Jentzen, W.; Unger, E.; Karvounis, G.; Shelnutt, J. A.; Dreybrodt, W.; Schweitzer-Stenner, R. *J. Phys. Chem.* **1996**, *100*, 14184. (c) Alden, R. G.; Ondrias, M. R.; Shelnutt, J. A. *J. Am. Chem. Soc.* **1990**, *112*, 691.

(9) Brennan, T. D.; Scheidt, W. R.; Shelnutt, J. A. *J. Am. Chem. Soc.* **1988**, *110*, 3919.

(10) Czernuszewicz, R. S.; Li, X.-Y.; Spiro, T. G. *J. Am. Chem. Soc.* **1989**, *111*, 7024.

(11) (a) Jentzen, W.; Song, X.-Z.; Turowska-Tyrk, I.; Scheidt, W. R.; Shelnutt, J. A. In preparation. During the preparation of this paper, the crystal structure of Ni(TPP) was obtained independently and reported, see: (b) Maclean, A. L.; Foran, G. J.; Kennedy, B. J.; Turner, P.; Hambley, T. W. *Aust. J. Chem.* **1996**, *49*, 1273. The reported structure is of the same space group and the bond lengths and bond angles are very close in the two structures. The reported displacements along the normal coordinates are from the structure of ref 11a.

(12) Shelnutt, J. A. *J. Phys. Chem.* **1983**, *87*, 605.

(13) (a) Torkington, P. *Appl. Spectrosc.* **1980**, *34*, 189. (b) Arora, A. K.; Umadevi, V. *Appl. Spectrosc.* **1982**, *36*, 424.

(14) For describing the nonbonding interactions, the Lennard-Jones 12-6 type expression was used except for hydrogen atoms for which the exponential-6 type expression was used. For the electrostatic (Coulombic)

interactions result from monopole−monopole interactions of partial atomic charges, see: Rappé, A. K.; Goddard, W. A., III. *J. Phys. Chem.* **1991**, *95*, 3358.

(15) The macrocyclic structure obtained from just the out-of-plane normal deformations of the saddling (*sad*, B_{2u}, 65 cm^{-1}), ruffling (*ruf*, B_{1u}, 88 cm^{-1}), doming (*dom*, A_{2u}, 135 cm^{-1}), waving [*wav*(*x*), *wav*(*y*); E_g, 176 cm^{-1}], and propellering (*pro*, A_{1u}, 335 cm^{-1}) types simulates the out-of-plane distortion of the X-ray crystal and energy-minimized structures. Similarly, the in-plane distortions are decomposed into in-plane normal deformations corresponding to the lowest-frequency vibrational modes including macrocycle stretching in the direction of the *meso*-carbon atoms (*meso-str*, B_{2g}, 213 cm^{-1}), stretching in the direction of the nitrogen atoms (*N-str*, B_{1g}, 260 cm^{-1}), *x*- and *y*-pyrrole translations [*trn*(*x*), *trn*(*y*); E_u, 360 cm^{-1}], macrocycle breathing (*bre*, A_{1g}, 367 cm^{-1}), and pyrrole rotation (*rot*, A_{2g}, 539 cm^{-1}) (ref 2).

(16) Generally, the mean positional error for the X-ray crystal structures of synthetic porphyrins in three dimensions is about 0.006 Å when the final refinement factor (*R*-value) is 0.07. However, in one (out-of-plane) and two (in-plane) dimensions, these errors are about 0.003 and 0.005 Å, respectively, assuming a Gaussian-distributed probability density function for the deviations (ref 2).

(17) Li, X.-Y.; Czernuszewics, R. S.; Kincaid, J. R.; Su, Y. O.; Spiro, T. G. *J. Phys. Chem.* **1990**, *94*, 31.

(18) (a) Yamamoto, T.; Palmer, G.; Gill, D.; Salmeen, I. T.; Rimai, L. *J. Biol. Chem.* **1973**, *248*, 5211. (b) Spiro, T. G.; Strekas, T. C. *J. Am. Chem. Soc.* **1974**, *96*, 338. (c) Kitagawa, T.; Ogoshi, H.; Watanabe, E.; Yoshida, Z. *J. Phys. Chem.* **1975**, *79*, 2629. (d) Spaulding, L. D.; Chang, C. C.; Yu, N.-T.; Felton, R. H. *J. Am. Chem. Soc.* **1975**, *97*, 2517. (e) Stong, J. D.; Spiro, T. G.; Kubaska, R. J.; Shupack, S. I. *J. Raman Spectrosc.* **1980**, *9*, 312. (f) Parthasarathi, N.; Hansen, C.; Yamaguchi S., Spiro, T. G. *J. Am. Chem. Soc.* **1987**, *109*, 3865. (g) Prendergast, K.; Spiro, T. G. *J. Am. Chem. Soc.* **1992**, *114*, 3793.

(19) Jentzen, W. Ph.D. Thesis, University of Bremen, Germany, Jan 1994.

(20) Jentzen, W.; Shelnutt, J. A. Unpublished results.

(21) Li, X.-Y.; Czernuszewicz, R. S.; Kincaid, J. R.; Stein, P.; Spiro, T. G. *J. Phys. Chem.* **1990**, *94*, 47.

(22) (a) Unger, E. Ph.D. Thesis, University of Bremen, Germany, May 1996. (b) Unger, E.; Dreybrodt, W.; Schweitzer-Stenner, R. In preparation.

(23) The optimum metal−nitrogen distance for planar metalloporphyrins is thought to be about 2.01 Å, see: Hoard, J. L. *Science* **1971**, *174*, 1295 and Hoard, J. L. *Ann. N. Y. Acad. Sci*. **1973**, *206*, 18. Upon comparing the metal-nitrogen distances of recently crystallized X-ray crystal structures of metalloporphines (ref 7), copper porphyrins best fulfill this condition.

(24) Li, X.-Y. Ph.D. Thesis, Princeton University, Oct 1988.

(25) The effect of the phenyl orientations on the frequencies of the phenyl modes can be studied by comparing the single-crystal Raman spectra of two X-ray crystal structures of Cu(TPP). Cu(TPP) can be crystallized in either a primarily ruffled (1.183 Å) or a saddled (−1.915 Å) conformation, see: Fleischer, E. B.; Miller, C. K.; Webb, L. E. *J. Am. Chem. Soc.* **1964**, *86*, 2342; Erler, B. S.; Scholz, W. F.; Lee, Y. J.; Scheidt, W. R.; Reed, C. A. *J. Am. Chem. Soc.* **1987**, *109*, 2644. Both crystal structures exhibit the *LRLR* phenyl orientations, but the dihedral angle between the phenyl and $C_\alpha C_m C_\alpha$ plane are much different. In one case the average angle is 81° and in the other case it is 52°.

(26) (a) Ziergski, M. Z.; Pawlikowski, M. *Chem. Phys.* **1982**, *65*, 335. (b) Schweitzer-Stenner, R.; Bobinger, U.; Dreybrodt, W. *J. Raman Spectrosc.* **1991**, *22*, 65. (c) Schweitzer-Stenner, R.; Stichternath, A.; Dreybrodt, W.; Jentzen, W.; Song, X.-Z.; Shelnutt, J. A.; Nielsen, O. F.; Medforth, C. J.; Smith, K. M. *J. Chem. Phys.* **1997**. In press.